Journal of ELECTRONIC MATERIALS, Vol. 49, No. 9, 2020
https://doi.org/10.1007/s11664-020-08267-8

Comprehensive Study on Nebulizer-Spray-Pyrolyzed Eu-Doped PbS Thin Films for Optoelectronic Applications

K. PAULRAJ,[1] S. RAMASWAMY,[2,6] S. SARAVANAKUMAR,[3] MOHD SHKIR,[4,7] S. ALFAIFY,[4] and ASLAM KHAN[5,8]

1.—Department of Physics, Pasumpon Muthuramalinga Thevar College, Usilampatti, Tamil Nadu 625532, India. 2.—PG and Research Department of Physics, N.M.S.S. Vellaichamy Nadar College, Nagamalai, Madurai, Tamil Nadu 625 019, India. 3.—Department of Physics, Kalasalingam Academy of Research and Education, Krishnankoil, Virudhunagar, Tamil Nadu 626126, India. 4.—Advanced Functional Materials and Optoelectronics Laboratory (AFMOL), Department of Physics, College of Science, King Khalid University, Abha 61413, Saudi Arabia. 5.—King Abdullah Institute for Nanotechnology, King Saud University, Riyadh 11451, Saudi Arabia. 6.—e-mail: ramaswamysvn@gmail.com. 7.—e-mail: shkirphysics@gmail.com. 8.—e-mail: aslamkhan@ksu.edu.sa

PbS films in undoped state and with various Eu contents (1 wt.%, 3 wt.%, and 5 wt.%) have been coated effectively on insulating glass substrates by a nebulized spray pyrolysis route. The effects of Eu doping on various properties including the photosensitivity of the PbS films were systematically analyzed. X-ray diffraction (XRD) analysis of the materials revealed a polycrystalline nature with crystallites showing simple cubic structure oriented along (200) direction. Based on the XRD data, the crystallite size, dislocation density, and lattice strain of the films with different doping concentrations were calculated and are consistently discussed. The secondary phase Eu_3O_4 formed when the Eu doping level was higher in the host solution. The Raman peaks detected at 190 cm^{-1}, 236 cm^{-1}, and 465 cm^{-1} confirmed formation of PbS. Scanning electron microscopy was used to reveal the morphology of the films as a function of the dopant concentration. Important optical properties including the bandgap, absorption coefficient, dielectric constant, index of refraction, and coefficient of extinction of the films are systematically reported. Optical study of the films revealed a variation of the bandgap from 2.14 eV to 2.81 eV with increasing Eu doping level. The 3 wt.% europium-doped PbS film showed better photosensitivity at 100 W/m^2 compared with the other films based on current–voltage (I–V) measurements.

Key words: Eu-doped PbS thin films, surface analysis, optical bandgap, photosensitivity studies

INTRODUCTION

A review of the literature reveals that semiconducting materials have been used in many technological and commercial devices because of their potential applications. Lead sulfide (PbS) is a vital semiconductor which is attractive for various applications due to its narrow bandgap of ~ 0.41 eV at 300 K and large exciton Bohr radius of 18 nm to 20 nm. Typically, PbS is a p-type compound with face-centered cubic (fcc) crystal system in the category of group II–VI semiconductors.[1–3] The direct bandgap of PbS material results in suitable absorption coefficient behavior from the visible to infrared (IR) region. PbS can be prepared as large-area thin films using various simple methods. Moreover, its properties depend on the growth conditions and nature of the substrate, and it has a variety of applications including infrared detectors,[4]

(Received February 29, 2020; accepted June 10, 2020; published online June 30, 2020)

photothermal solar energy conversion,[5] field-effect transistors,[6] radiation control coatings,[7,8] decorative coatings,[9,10] and various sensors.[11,12] The photosensitivity of lead chalcogenide films is influenced by the film thickness, grain size, number of layers, temperature, and impurities. The photoelectric properties of lead sulfide can be affected by changing the bandgap structure, altering the photoresponse, as well as doping with appropriate elements.[13] Blount et al.[14] and Kothiyal et al.[15] studied and reported the effect of the grain size and topography of the films on their photoresponse. Various nanostructured PbS films have been prepared by numerous methods including electrodeposition,[16] the sonochemical route,[17] spray pyrolysis,[18] successive ionic layer adsorption and reaction (SILAR),[19] and the sol–gel method.[20] Amongst these, spray pyrolysis is a low-cost and simple method that does not require any complicated or costly equipment. Therefore, in this work, the nebulizer spray pyrolysis (NSP) method was employed to obtain doped and undoped PbS thin films. Doping is an effective way to alter or improve the properties of a material to make it suitable for specific applications. Recently, many works have been reported on doping of PbS ceramics with different metals,[21–24] but further exploration is required to prepare high-quality PbS films with good physicochemical properties.

Moreover, rare-earth metals have the capability to absorb light at shorter wavelengths and emit it at higher wavelengths.[21] Various rare-earth elements (Eu, Gd, Nd, Yi, Sm, and Pr) are highly suitable dopants for group II–VI semiconductors.[25] Amongst these, europium (Eu) is a useful metal, as it can effortlessly adapt to the PbS structure to achieve good optical properties while the Eu ions can be used as down-shifting layers in the electronic band structure. Gollakota et al.[26] formed a practical red-light emitter on glass by creating an Eu-doped Ga_2O_3 light-emitting layer that was optically transparent across the visible region. Hao et al.[27] observed that the strongest line corresponded to the $^5D_0$–$^7F_2$ electronic transition in the electroluminescence of spray-coated Ga_2O_3 thin films with Eu^{3+} doping. Masuda et al.[28] developed a visible-light-emitting Eu-doped Y_2O_3 film on self-assembled monolayers that showed red emission (611 nm). Garcıa-Murillo et al.[29] observed the fluorescence decay properties due to the presence of the two sites known for Eu^{3+} in cubic Gd_2O_3. Domaradzk et al.[30] presented an enhancement of the photocatalytic properties of TiO_2:Eu thin films by adding more hydroxyl species at the surface of the Eu-doped thin films. Thus, Eu^{3+} ions can effectively participate in energy-transfer luminescent and result in more hydroxyl species for photocatalytic activity. Considering these advantages, europium (Eu) was used in this work as a dopant to obtain PbS:Eu films by the simple NSP method, and their structural, morphological, optical, and photoresponse characteristics were studied.

EXPERIMENTAL PROCEDURES

Film Casting

High-quality PbS:Eu films were systematically deposited by a simple NSP technique on cleaned glass substrates. To prepare undoped PbS thin film, analytical-grade lead nitrate ($PbNO_3$) and thiourea [CS $(NH_2)_2$] were used as reaction materials. Europium doping was achieved using analytical-grade europium chloride hexahydrate ($EuCl_3{\cdot}6H_2O$) at different concentrations. Before deposition of the films, a cleaning process was carried out and the solution for spraying was prepared using a $PbNO_3$:thiourea ratio of 1:1 in about 10 ml of double-distilled water. To deposit the films, the temperature of the substrate was kept at 220°C (±2 °C accuracy) and the solution was sprayed either undoped or with 1 wt.%, 3 wt.%, or 5 wt.% Eu doping. A distance of 50 mm was maintained between the substrate and spray nozzle. After deposition, the prepared PbS and PbS:Eu films were further characterized.

Characterization

The prepared PbS and PbS:Eu films were analyzed using various techniques to identify their structure, morphology, composition, and optoelectrical properties. The structural properties of the prepared Eu-doped PbS thin films were analyzed by XRD (Shimadzu X-600) with Cu K_α radiation over the angular range from 10° to 80°. The surface morphology was imaged using a JSM 7600 F (JEOL, Japan). The fabricated films were subjected to Raman spectroscopy using a DXR spectrometer using a laser at λ_{exc} = 532 nm with power of 5 mW. Their optical properties were evaluated using a JASCO-V570 UV–Vis spectrophotometer in the range from 300 nm to 2500 nm. A PerkinElmer LS 45 fluorescence spectrophotometer was employed to record their PL emission spectra. The electrical photosensitivity of the prepared samples was analyzed using a Keithley model-2450. The film thickness was calculated using a stylus profilometer (Table I).

RESULTS AND DISCUSSION

Structural Studies

To examine the structural changes in the synthesized PbS:Eu thin films, their structure was analyzed using an appropriate XRD method. Figure 1 depicts the detailed x-ray diffraction profiles of all the PbS:Eu films with different Eu concentrations (0 wt.%, 1 wt.%, 3 wt.%, and 5 wt.%). This figure clearly shows that all the deposited films exhibited five well-defined characteristic peaks for (111), (200), (220), (311), and (400), showing good

Table I. Structural parameters of PbS thin films deposited with various Eu doping concentrations

Eu doping concentration (%)	Film thickness (nm)	Crystallite size (nm)	Dislocation density ($\delta \times 10^{14}$ lines m^{-2})	Strain $\varepsilon \times 10^{-3}$	Texture Coefficient (TC) (*hkl*)
0	500	21	2.20	6.28	1.17
1	530	22	2.11	6.17	1.22
3	560	24	1.76	5.61	1.36
5	540	23	1.78	5.63	1.32

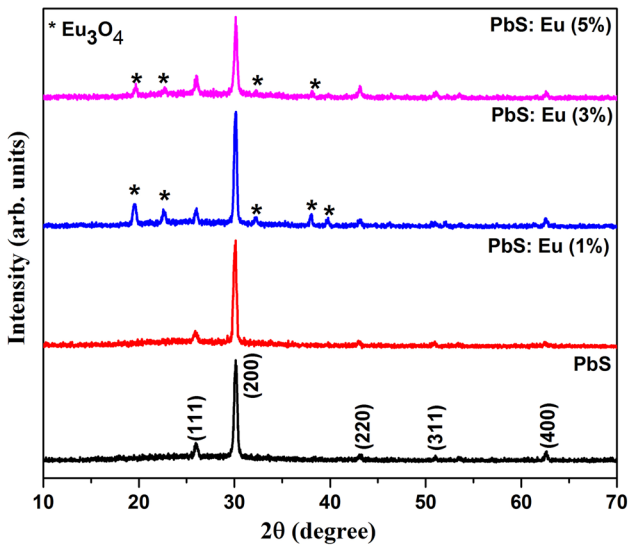

Fig. 1. XRD patterns of undoped and Eu-doped PbS thin films.

agreement with typical peaks for PbS in Joint Committee on Powder Diffraction Standards (JCPDS) File No. 05-0592 and thus corresponding to the PbS lattice. Also, the films showed polycrystalline nature. Among the five characteristic peaks, that corresponding to (200) plane was stronger than the others, indicating the preferential growth direction of the films. Puiso et al.[19] and Gadave et al.[31] also observed the same type of preferential orientation along (200) plane. The other four peaks were narrow, being assigned to (111), (220), (311), and (400) planes. The purity of PbS was not reduced up to Eu doping concentration of 1% as no peaks associated with Eu were observed. Similarly, monophase polycrystalline nature were also observed by Zheng et al.[32] for Cu-doped PbS films. Furthermore, it is apparent that Eu_3O_4 phase was observed in the PbS films doped with 3 wt.% and 5 wt.% europium concentrations due to placement of Eu^{3+} ions interstitially rather than substitutionally. The observed Eu_3O_4 peaks are in agreement with JCPDS card no. 86-2476. Moreover, note that, with increasing Eu content, the intensity of the signal from (200) plane increased up to 3% concentration, indicating an improvement in the crystallinity of the PbS lattice. Furthermore, for the 5 wt.% Eu concentration, the peak intensity decreased, which might be due to structural disorder in the crystal structure. The ionic radius plays a crucial role in lattice disorder: if the ionic radius of the dopant is higher than or equal to that of the host material, it may result in some unusual lattice formation and thus reduce the purity of the structure. Here, the ionic radius of Eu^{3+} (0. 96 Å) is almost equal to that of Pb^{2+} (1.19 Å); however, with increasing doping level, it may still produce lattice alteration/crystal deficiencies and thus disrupt the crystalline perfection of the host Pb^{2+}. Ravisankar et al.[33] reported such a peak reduction of the host PbS film with increasing Gd doping concentration.

The crystallite size (D) was estimated using the measured x-ray parameter values of (200) plane by applying Scherrer's equation[34,35]

$$D = \frac{0.9\lambda}{\beta \cos\theta}, \tag{1}$$

where λ is the wavelength (1.5406 Å), β is the full-width at half-maximum (FWHM) for (200) peak, and θ is the angular position. Note that the estimated D value increased from 21 nm to 24 nm as the Eu content was increased from 0 wt.% to 3 wt.% owing to a decrease of the FWHM values. The crystallinity of the PbS films improved up to 3 wt.% Eu doping with decreasing microstrain and dislocation density. This may reduce the lattice imperfections around grain boundaries.[36] For the highest Eu doping percentage (5 wt.%), the crystallite size reduced suddenly; this might be due to excess Eu ions occupying interstitial positions.

The structural parameters such as the microstrain (ε) and defect density (δ) were calculated using the following equations [37–39]:

$$\varepsilon = \frac{\beta \cot\theta}{4}, \tag{2}$$

$$\delta = \frac{1}{D^2}. \tag{3}$$

A good semiconducting compound film should exhibit lower ε and δ values. The variation of the ε and δ values of the films is presented in Table I. Low ε and δ values of 0.0056 lines^{-2} m^{-4} and 0.17 $\times$ 10^{15} nm^{-2}, respectively, were obtained for the 3%

Eu-doped PbS film. This reflects an increase in the lattice defect concentration as Eu ions are placed substitutionally in PbS. The texture coefficient is one of the basic structure parameters, being calculated using the equation[40]

$$TC(hkl) = \frac{I(hkl)/I_0(hkl)}{N_r^{-1}\sum I(hkl)/I_0(hkl)}, \quad (4)$$

where $I(hkl)$ and $I_0(hkl)$ are the recorded and typical intensities, while N_r is the observed reflection number of the diffraction peaks. Table I presents the TC values as a function of Eu content. The TC values increased with growing Eu content due to the increase in phonon scattering. Note also that the sample with 3% doping showed the maximum texture coefficient value of 1.36. Typically, a TC value greater than one (TC > 1) indicates abundant grains in the particular sample. In the current case, the calculated TC value was > 1 for all the deposited PbS:Eu films, suggesting that greater numbers of crystallites were assembled in the predominant (200) plane, as also evidenced by the XRD patterns.

Raman Study

Raman spectroscopy is an effective technique that can provide useful phase information about the vibrational modes of a material. As per group theory, crystalline PbS is assigned to space group Fm_3m.[41] Figure 2 shows the room-temperature Raman spectra of the undoped and PbS:Eu3% deposited films in the wavenumber region from 150 cm^{-1} to 600 cm^{-1}. An equal number of Raman peaks was observed for the undoped and PbS:Eu3% deposited films. According to Fig. 2, the undoped and 3.0 wt.% PbS:Eu films displayed Raman characteristic peaks at 190 cm^{-1}, 236 cm^{-1}, and 465 cm^{-1}. The major peak observed at ~ 190 cm^{-1} corresponds to the combination of longitudinal and transverse (LO–TO) optical modes.[42,43] The second peak observed at 236 cm^{-1} corresponds to the lowest-order phonon mode.[44,45] The peak observed at 465 cm^{-1}corresponds to the longitudinal optical phonon mode (2LO).[46] The Raman peak appearing at 465 cm^{-1} can be attributed to the LO phonon mode of the Brillouin zone. Moreover, the intensity of the peaks decreased with increasing Eu concentration up to 3 wt.% owing to lattice imperfections.

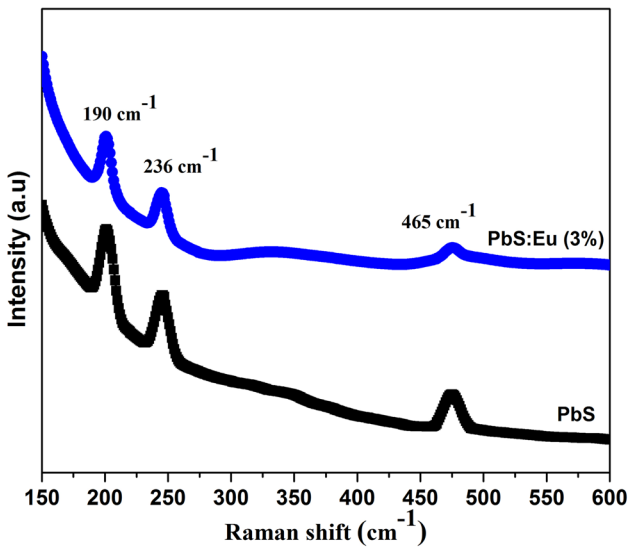

Fig. 2. Raman spectra of undoped and Eu-doped PbS thin films.

Morphological Study

Figure 3a–d shows FESEM images of the PbS:Eu films with different Eu contents, revealing a notable effect on the morphology of the PbS:Eu films in comparison with PbS. The undoped PbS film exhibited tightly packed nanosized grains spread over the entire surface, as seen in Fig. 3a and similar to an earlier report.[47] Figure 3b reveals the inhomogeneous granular structure of the precise grains on the surface of the 1 wt.% PbS:Eu film. It is obvious that, as the Eu doping concentration was increased, the surface topography of the coated PbS thin film was modified, with well-defined grains.[32] Besides, a reduction in the voids is also seen in Fig. 3c, where densely packed grains appear on the surface of the 3 wt.% Eu:PbS film. Moreover, the film deposited with 5 wt.% Eu content showed further modification of the surface, exhibiting some spherical-like grains with porous nature.

Elemental Analysis

Elemental analysis of the films was carried out by EDX. Figure 4 shows the EDX elemental mapping images for the 3 wt.% PbS:Eu thin film. The presence of Eu element was confirmed, as well as lead and sulfur. The incorporation of Eu is confirmed by the respective images. The EDX elemental spectra show that the host PbS structure containing lead and sulfur (red and blue) elements was clearly present and regular with no pinholes, as well as the europium dopant (green). Furthermore, the violet color in these images indicates the combination of Pb, S, and Eu elements. Figure 5 illustrates the elemental composition according to the EDX spectrum of the same film. These spectra confirm the presence of the expected elements Pb, S, and Eu in the 3% Eu-doped PbS film. The elemental composition of the PbS:Eu system was nearly stoichiometric with 48.1% Pb, 49.1% S, and 2.8% Eu. As expected, no other peaks were detected in the deposited films, confirming the purity of the PbS:Eu materials deposited by the NSP method.

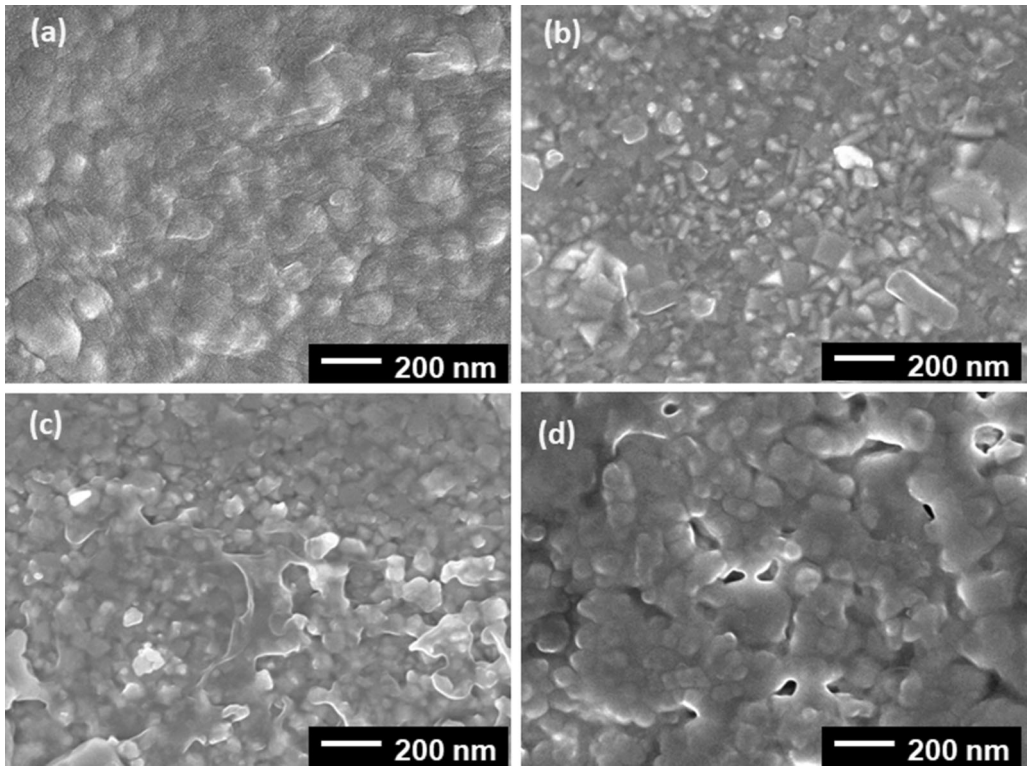

Fig. 3. SEM images of PbS thin films: (a) undoped, and doped with (b) 1 wt.%, (c) 3 wt.%, and (d) 5 wt.% Eu.

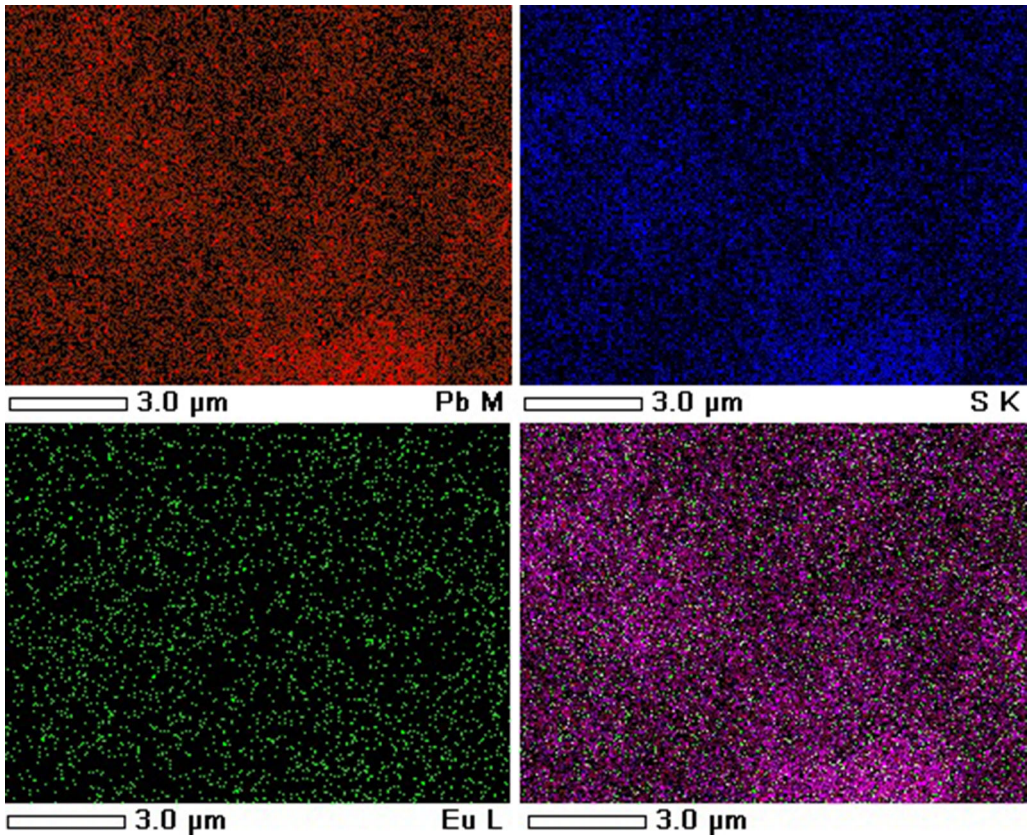

Fig. 4. Elemental mapping of 3 wt.% Eu-doped PbS film.

Optical Analysis

To understand the effect of Eu doping on the PbS films in terms of their optical absorbance and transmittance, optical data were recorded in the UV to IR region. Figure 6a shows that the transmittance of the PbS films was high in the visible region and increased with rising Eu doping content. The reason for the increasing transmittance may be the low scattering effect in the samples.[48–50] Figure 6b shows the absorption spectra of the deposited films, revealing a noticeable decrease with increasing Eu concentration. This decrease in absorbance can be attributed to the decreasing thickness of the samples.[51] From these two spectrum, the vertical absorption edge shifted toward lower wavelengths, corresponding to an increase in the bandgap, with increasing Eu doping level. The same kind of effect on the absorption edge was observed by Merino et al.[52] for Hg-doped PbS films.

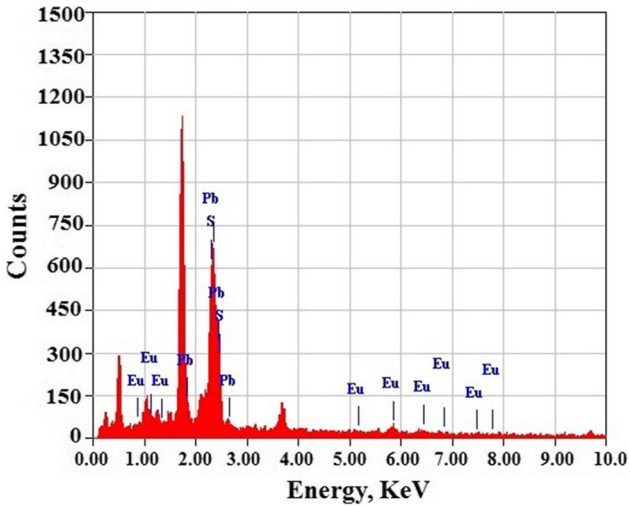

Fig. 5. EDX spectrum of 3 wt.% Eu-doped PbS film.

The optical energy gap of the films was obtained from Tauc's relation[53]:

$$\alpha h\nu = B(h\nu - E_g)^n, \tag{5}$$

where all the symbols have their usual meanings. The E_g value of the Eu:PbS films (Fig. 6c) increased from 2.14 eV to 2.81 eV, showing good agreement with reported data.[50–52] Using Tauc's relation, bandgap values of 2.14 eV, 2.23 eV, 2.26 eV, and 2.81 eV were obtained for the samples with 0 wt.%, 1 wt.%, 3 wt.%, and 5 wt.% Eu, respectively. The bandgap depends on the blue-shift observed in the absorption spectrum, and these variations correspond to the change in the blue-shift phenomena as well as the quantization effect.[52] Moreover, the increment of the bandgap may be due to the decrease in the film thickness as well as the enhancement of the crystallite size. Such tuning of the energy gap of PbS:Eu film could have extensive technological applications in innovative solar cells.

The optical characteristics, viz. the refractive index (n) and extinction coefficient (k), were obtained from the reflectance and transmittance using the standard equations[54–56]:

$$n = \left(\frac{1+R}{1-R}\right) + \sqrt{\frac{4R}{(1-R)^2} - k^2}, \tag{6}$$

$$k = \frac{\alpha\lambda}{4\pi}. \tag{7}$$

The refractive index can provide useful information about the behavior of light for various technological applications. Figure 7 shows the plots of n and k for the Eu:PbS films. The calculated values are found to decrease with increasing Eu concentration, which can be attributed to the creation of lattice defects and crystalline disorder, which will

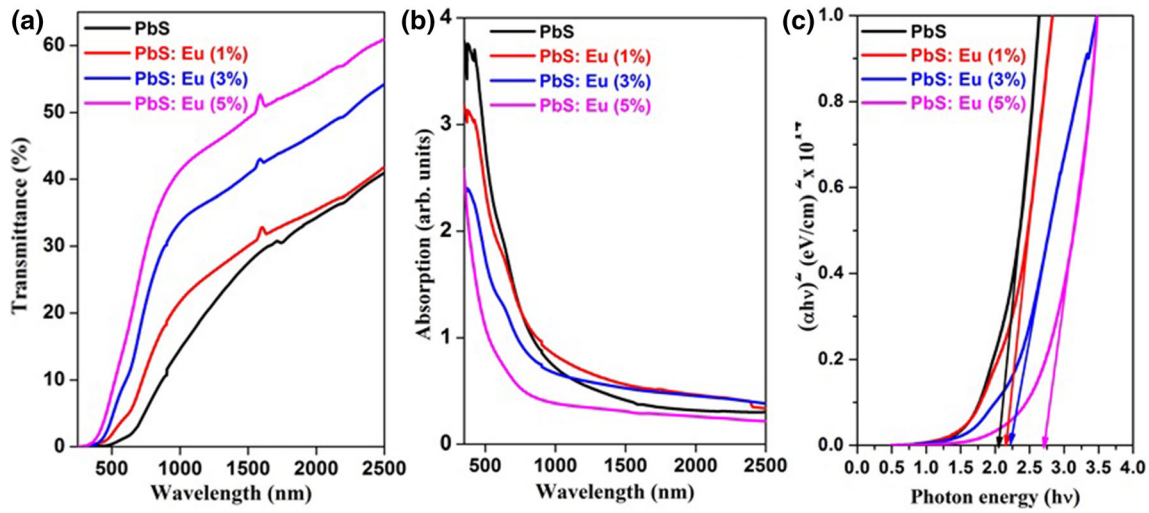

Fig. 6. (a) Transmittance and (b) absorption spectra and (c) ($h\nu$) versus $(\alpha h\nu)^2$ plot of Eu-doped PbS thin films.

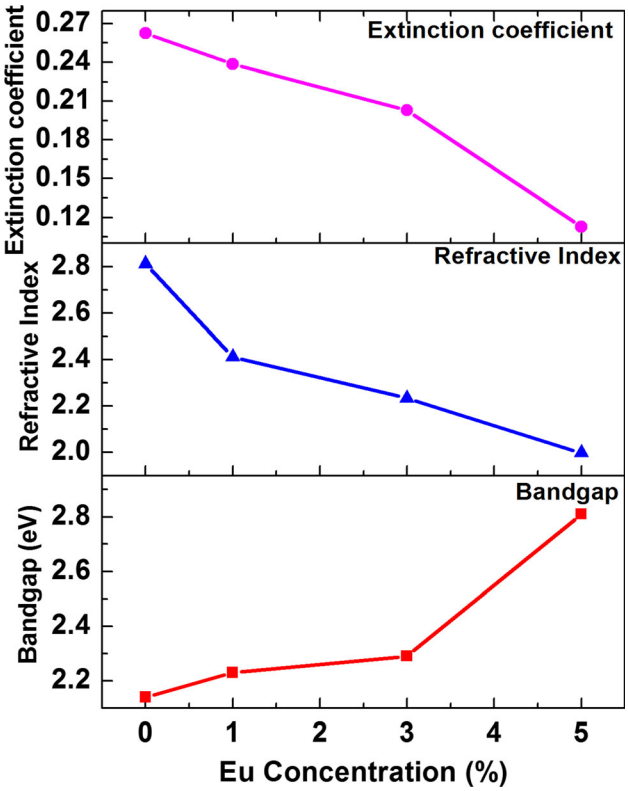

Fig. 7. Variation of bandgap, refractive index, and extinction coefficient of Eu-doped PbS thin films.

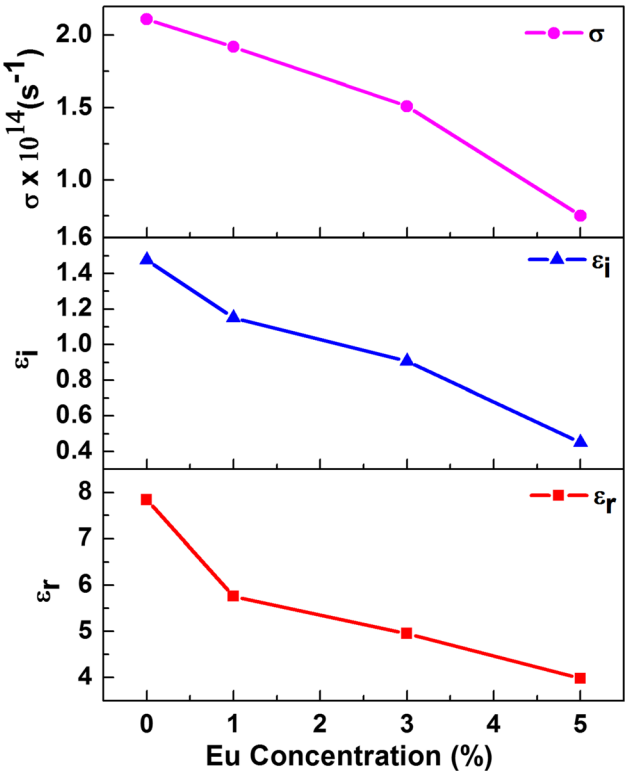

Fig. 8. Variation of real and imaginary parts of dielectric constant and optical conductivity of Eu-doped PbS thin films.

reduce the crystalline quality. The reduction of the refractive index can be ascribed to the light propagation through the prepared films. Consequently, the velocity of light might be increased, resulting in easy interaction with the surface of the prepared films and thereby enhancing their optical as well as electrical properties for technological applications. Low values of n and k of 1.96 and 0.11, respectively, were found for the 5% Eu-doped PbS film, indicating good transparency due to the enhancement of the bandgap.

The real (ε_r) and imaginary (ε_i) parts of the dielectric constant of the deposited films were estimated as[57]

$$\varepsilon_r = n^2 - k^2, \tag{8}$$

$$\varepsilon_i = 2nk. \tag{9}$$

Usually, ε_r and ε_i are used to measure the degree of wave dispersion and dissipation in the medium. These parameters can also describe the polarizability and capacitive control of devices. Figure 8 shows low dielectric constants, revealing a small capacitance and rapid response time of the prepared materials. Both dielectric constant values decreased with the Eu doping level due to the decrease in the film thickness as well as the enhanced uniformity of the crystallites. The optical conductivity was calculated using the equation

$$\sigma = \alpha nc/4\pi. \tag{10}$$

Figure 8 shows the optical conductivity of the pure sample and those doped with different concentrations of Eu. This figure reveals that the optical conductivity decreased with increasing Eu doping due to the increasing photon energy values as evidenced in the bandgap spectra. The reason for this decrease in the optical conductivity may be due to the low absorption coefficient of lead sulfide thin films as well as excitation of electrons by the photon energy.

Photoluminescence Studies

The PL emission (PLE) spectra of the PbS and 3 wt.% Eu-doped PbS films are shown in Fig. 9. The PLE spectra were obtained by exciting the films at 325 nm, with a main band at $\sim 550 \pm 4$ nm (green) assigned to near-band-edge (NBE) emission due to V_{Pb}/intrinsic defects occurring through grain growth.[54] The PLE band was observed at ~ 546 nm for the 3 wt.% PbS:Eu film. Quenching of the PLE band intensity was noticed, along with a blue-shift. Such quenching of the PLE band intensity implies a reduction in the crystallinity of the PbS film on Eu doping and decreased defect formation. The blue-shift of the PLE band is also related to the variation of the bandgap in PbS:Eu.

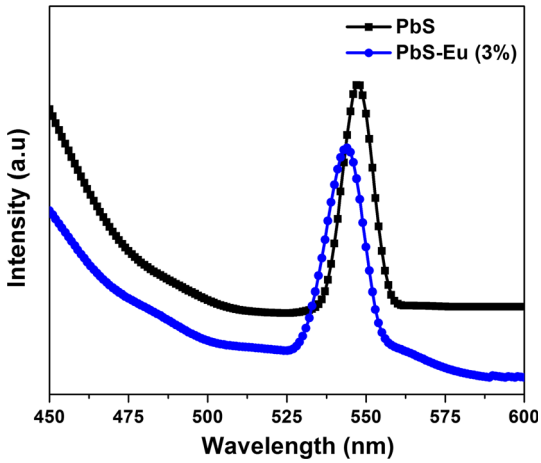

Fig. 9. PL spectra of undoped and 3 wt.% Eu-doped PbS thin films.

Photosensitivity *I–V* Studies

A schematic of the Eu-doped PbS:Eu thin film coated on the glass substrate is shown in Fig. 10a. The photocurrent switching characteristic of the film under a constant bias voltage of 10 V is shown in Fig. 10b. Note that the rise time and decay time of PbS:Eu (3 wt.%) were 1 s and 9 s, respectively. These results are highly comparable to those of Kim et al.,[58] who reported the photocurrent decay time for chemical vapor deposition (CVD)-grown PbS nanowires. The responsivity (R) is expressed as $R = (I_{light} - I_{dark})/P_{inc}$, where I_{light} is the signal under illumination, I_{dark} is the dark current, and P_{inc} is the power of the light incident on the active area. Iacovo et al.[59] reported an R value of $\sim$ 30 A W^{-1} at a bias voltage of 1 V. Wei et al.[60] reported R values for organic and PbS photodetectors of $\sim$ 0.75 A W^{-1} and 0.19 A W^{-1}, respectively, and an improvement of R to 1.89 A W^{-1} for the bilayer. Tang et al.[61] noted an enhancement

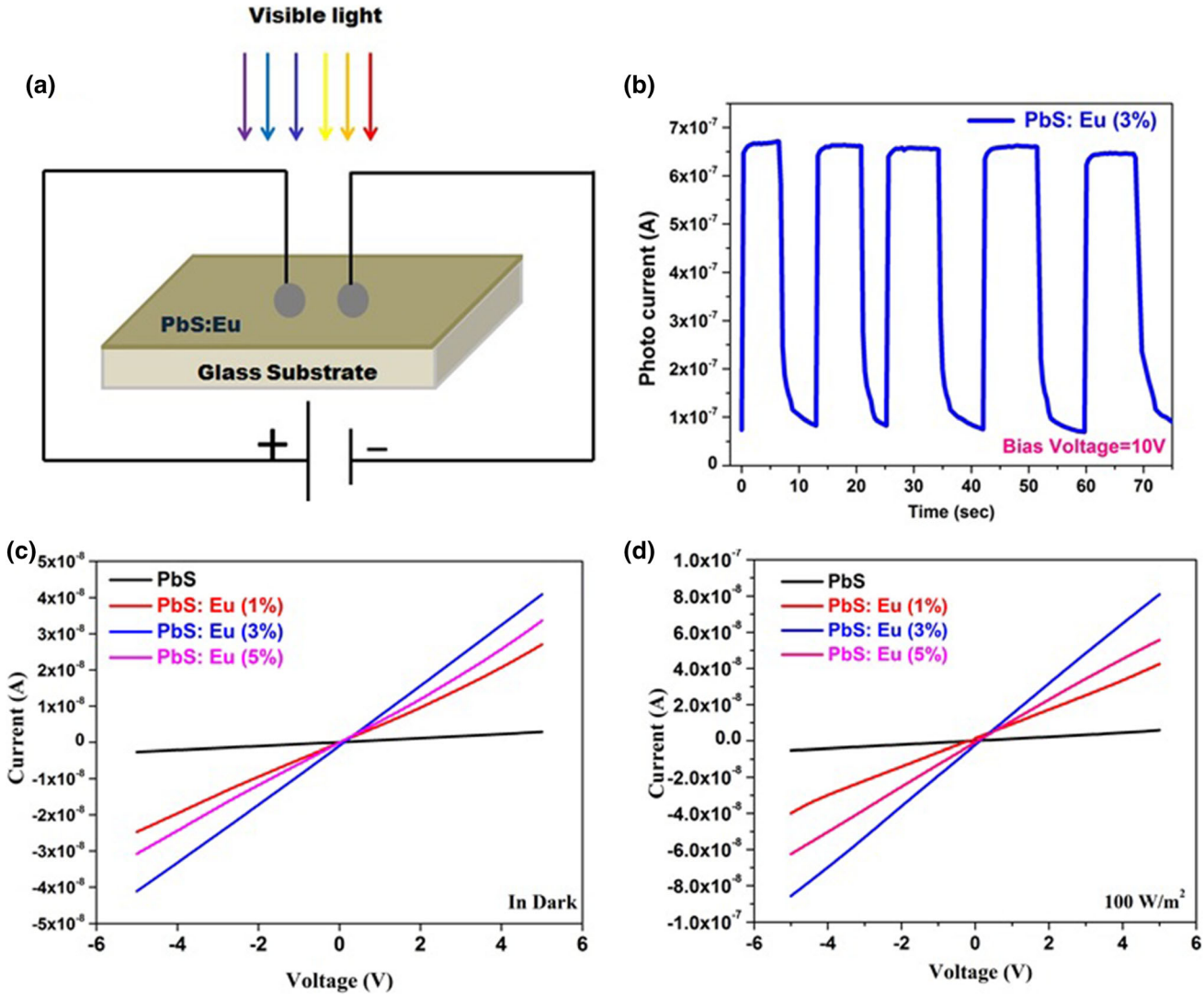

Fig. 10. (a) Schematic diagram, (b) photocurrent versus time, and current–voltage characteristic curve in (c) dark and (d) illuminated condition for PbS and Eu-doped PbS thin films.

in R of 94% for a photodetector constructed from PbS quantum dots (QDs). Meanwhile, in the current work, we found an R value of ~ 5 A W^{-1} when the europium content in the PbS matrix was 3 wt.%, which is somewhat higher compared with the result reported by Wei et al. The photosensing properties of the PbS:Eu films were measured both in the dark and under illumination at 100 W/m^2 using Ag as a metal contact. The current in the dark recorded between -5 to $+5$ V for PbS and PbS:Eu is depicted in Fig. 10c, confirming the ohmic nature of the fabricated films. The value of I increased until 3 wt.% of Eu, but decreased slightly thereafter. The I–V plots obtained under light illumination are shown in Fig. 10d, clearly revealing an increase in the I value for Eu-doped PbS. This enhancement of the I value may be due to the creation of extra electron–hole pairs when light of appropriate energy is incident on the films, which breaks the bond in the PbS:Eu semiconductor. Based on the results of this study, the 3% Eu-doped PbS film showed good photosensing behavior and is well suited for use in energy-based devices.

CONCLUSION

Device-grade Eu-doped PbS films were prepared by the NSP technique. XRD analysis revealed their polycrystalline nature and indicated D values varying from 21 nm to 24 nm with increasing Eu doping concentration. The high mode peak at 190 cm^{-1} observed in Raman analysis indicated LO-TO optical modes of the PbS crystal structure. XRD and EDX studies confirmed successful incorporation of europium into the PbS structure. SEM confirmed the agglomeration of grains that were well organized on the film surface. The optical bandgap increased as the Eu doping concentration was increased. Photosensitivity analysis confirmed an increase of the current and voltage levels under light illumination. The prepared PbS:Eu films could be used in technological applications, e.g., as the absorber layer in photovoltaic devices, due to their light conducting behavior. Based on the results of this study, solar cell, light-emitting diode (LED), and luminescence-related devices could be further fabricated in the future.

ACKNOWLEDGMENTS

The authors would like to express their gratitude to Deanship of Scientific Research at King Khalid University, Saudi Arabia for funding this work through Research Groups Program under Grant No. R.G.P.1/207/41. A.K. acknowledges the Researchers Supporting Project (RSP-2019/127), King Saud University, Riyadh, Saudi Arabia for financial support.

CONFLICT OF INTEREST

The authors declare that they have no conflicts of interest.

REFERENCES

1. A.N. Banerjee, *Nanotechnol. Sci. Appl.* 4, 35 (2011).
2. E. Yücel, Y. Yücel, and B. Beleli, *J. Alloys Compd.* 642, 63 (2015).
3. E. Yücel, Y. Yücel, and B. Beleli, *J. Cryst. Growth* 422, 1 (2015).
4. J.H. Warner, N. Heckenberg, and H. Rubinsztein-Dunlop, *Mater. Lett.* 60, 3332 (2006).
5. B.K. Gupta, R. Thangaraj, and O.P. Agnihotri, *Sol. Energy Mater.* 1, 481 (1979).
6. V.L. Colvin, M.C. Schlamp, and A.P. Alivisatos, *Nature* 370, 354 (1994).
7. I. Pop, C. Nascu, V. Ionescu, E. Indrea, and I. Bratu, *Thin Sol. Films* 307, 240 (1997).
8. H. Hirata and K. Higashiyama, *Bull. Chem. Sci. Jpn.* 44, 2420 (1971).
9. P. Nair, V. Garcia, A. Hernandez, and M. Nair, *J. Phys. D Appl. Phys.* 24, 1466 (1991).
10. S. Pawar, J. Shaikh, R. Devan, Y. Ma, D. Haranath, P. Bhosale, and P. Patil, *Appl. Surf. Sci.* 258, 1869 (2011).
11. T. Fu, *Sens. Actuators B Chem.* 140, 116 (2009).
12. X. Shen, Z. Li, Y. Cui, and Y. Pang, *Int. J. Electrochem. Sci.* 6, 3525 (2011).
13. R. Tyagi, S. Agarwal and V. Sethi, *Electrical and Optical-Properties of Chemically Sprayed Lead Sulfide Films*, Council Scientific Industrial Research Publ & Info Directorate, New Delhi City, p. 670 (1977).
14. G.H. Blount, P.J. Schreiber, D.K. Smith, and R.T. Yamada, *J. Appl. Phys.* 44, 978 (1973).
15. G. Kothiyal and B. Ghosh, *Prog. Cryst. Growth Charact. Mater.* 20, 313 (1990).
16. Y.J. Yang, *Mater. Sci. Eng. B* 131, 200 (2006).
17. Z. Xiu, S. Liu, J. Yu, F. Xu, W. Yu, and G. Feng, *J. Alloys Compd.* 457, L9 (2008).
18. B. Thangaraju and P. Kaliannan, *Semicond. Sci. Technol.* 15, 849 (2000).
19. J. Puišo, S. Lindroos, S. Tamulevičius, M. Leskelä, and V. Snitka, *Thin Solid Films* 428, 223 (2003).
20. A. Martucci, J. Fick, S.-É. LeBlanc, M. LoCascio, and A. Haché, *J. Non-Cryst. Solids* 345–346, 639 (2004).
21. S.R. Rosario, I. Kulandaisamy, K.D.A. Kumar, K. Ramesh, H.A. Ibrahium, and N.S. Awwad, *Int. J. Energy Res.* 44, 4505 (2020).
22. S.R. Rosario, I. Kulandaisamy, A.M.S. Arulanantham, K.D.A. Kumar, S. Valanarasu, M.S. Hamdy, K.S. Al-Namshah, and A.M. Alhanash, *Mater. Res. Exp.* 6, 056201 (2019).
23. M. Shkir, K.V. Chandekar, A. Khan, A.M. El-Toni, and S. AlFaify, *Mater. Sci. Semicond. Proc.* 107, 104807 (2020).
24. M. Shkir, M.T. Khan, A. Khan, A.M. El-Toni, A. Aldalbahi, and S. AlFaify, *Mater. Sci. Semicond. Proc.* 96, 16 (2019).
25. P. Wellenius, A. Suresh, J.V. Foreman, H.O. Everitt, and J.F. Muth, *Mater. Sci. Eng. B* 146, 252 (2008).
26. P. Gollakota, A. Dhawan, P. Wellenius, L.M. Lunardi, J.F. Muth, Y.N. Saripalli, H.Y. Peng, and H.O. Everitt, *Appl. Phys. Lett.* 88, 221906 (2006).
27. J. Hao, Z. Lou, I. Renaud, and M. Cocivera, *Thin Solid Films* 467, 182 (2004).
28. Y. Masuda, M. Yamagishi, and K. Koumoto, *Chem. Mater.* 19, 1002 (2007).
29. A. Garcia-Murillo, C. LeLuyer, C. Garapon, C. Dujardin, E. Bernstein, C. Pedrini, and J. Mugnier, *Opt. Mater.* 19, 161 (2002).
30. J. Domaradzki, D. Kaczmarek, A. Borkowska, D. Schmeisser, S. Mueller, R. Wasielewski, A. Ciszewski, and D. Wojcieszak, *Vacuum* 82, 1007 (2008).
31. K.M. Gadave, S.A. Jodgudri, and C.D. Lokhande, *Thin Solid Films* 245, 7 (1994).
32. X. Zheng, F. Gao, F. Ji, H. Wu, J. Zhang, X. Hu, and Y. Xiang, *Mater. Lett.* 167, 128 (2016).
33. S. Ravishankar, A.R. Balu, and V.S. Nagarethinam, *J. Electron. Mater.* 47, 1271 (2018).
34. M. Shkir, Z.R. Khan, M. Anis, S.S. Shaikh, and S. AlFaify, *Chin. J. Phys.* 63, 51 (2020).

35. M. Shkir, I.M. Ashraf, S. AlFaify, A.M. El-Toni, M. Ahmed, and A. Khan, *Ceram. Int.* 46, 4652 (2019).
36. A. Singh, V. Viswanath, and V. Janu, *J. Lumin.* 129, 874 (2009).
37. T. Rattana, S. Suwanboon, P. Amornpitoksuk, A. Haidoux, and P. Limsuwan, *J. Alloys Comp.* 480, 603 (2009).
38. M. Ravikumar, R. Chandramohan, K.D.A. Kumar, S. Valanarasu, A. Kathalingam, V. Ganesh, M. Shkir, and S. AlFaify, *J. Sol-Gel. Sci. Technol.* 85, 31 (2018).
39. M. Shkir and S. AlFaify, *J. Mater. Res.* 34, 2765 (2019).
40. K.D.A. Kumar, V. Ganesh, S. Valanarasu, M. Shkir, I. Kulandaisamy, A. Kathalingam, and S. AlFaify, *Mater. Chem. Phys.* 212, 167 (2018).
41. R. Yousefi, M. Cheraghizade, F. Jamali-Sheini, W.J. Basirun, and N.M. Huang, *Curr. Appl. Phys.* 14, 1031 (2014).
42. F. Gode, O. Baglayan, and E. Guneri, *Chalcog. Lett.* 12, 519 (2015).
43. Y. Bencherif, A. Boukra, A. Zaoui, and M. Ferhat, *Infrared Phys. Technol.* 54, 39 (2011).
44. S.V. Bhatt, M. Deshpande, B.H. Soni, N. Garg and S.H. Chaki: Chemical bath deposition of lead sulphide (PbS) thin film and their characterization, in *Solid State Phenomena*, (vol. 209, Trans Tech Publ, City, 2014), p. 111.
45. J. Rivera-Nieblas, J. Alvarado-Rivera, M. Acosta-Enríquez, R. Ochoa-Landin, F. Espinoza-Beltrán, A. Apolinar-Iribe, M. Flores-Acosta, A. De Leon, and S. Castillo, *Chalcogenide Lett.* 10, 349 (2013).
46. R. Sherwin, R.J.H. Clark, R. Lauck, and M. Cardona, *Sol. State Commun.* 134, 565 (2005).
47. E. Sarica and V. Bilgin, *Mater. Sci. Semicond. Proc.* 68, 288 (2017).
48. A.M.S. Arulanantham, S. Valanarasu, K. Jeyadheepan, and A. Kathalingam, *Thin Solid Films* 666, 85 (2018).
49. E. Yücel and Y. Yücel, *Ceram. Int.* 43, 407 (2017).
50. C. Rajashree, A. Balu, and V. Nagarethinam, *J. Mater. Sci.: Mater. Electron.* 27, 7876 (2016).
51. G. Singh Lotey, Z. Jindal, V. Singhi, and N.K. Verma, *Mater. Sci. Semicond. Proc.* 16, 2044 (2013).
52. R. Palomino-Merino, O. Portillo-Moreno, L. Chaltel-Lima, R.G. Pérez, M. de Icaza-Herrera, and V. Castaño, *J. Nanomater.* 2013, 45 (2013).
53. J. Tauc, R. Grigorovici, and A. Vancu, *Phys. Stat. Sol.* 15, 627 (1966).
54. T. Moss, G.J. Burrell, and B. Ellis, *Semiconductor Opto-Electronics* (London: Butterworth-Heinemann, 1959).
55. M. Arif, M. Shkir, S. AlFaify, A. Sanger, P.M. Vilarinho, and A. Singh, *Opt. Laser Technol.* 112, 539 (2019).
56. Y. Gülen, *Metall. Mater. Trans. A* 46, 4698 (2015).
57. M. Shkir, M.T. Khan, and S. AlFaify, *Appl. Nanosci.* 9, 1417 (2019).
58. J. Kim, E. Oh, R. Xiao, S. Ritter, Y. Yang, D. Yu, J. HeeIm, S. HyukKim, W. JunChoi, and J.-G. Park, *Nanotechnology* 28, 475706 (2017).
59. A. De Iacovo, C. Venettacci, L. Colace, L. Scopa, and S. Foglia, *Sci. Rep.* 6, 1 (2016).
60. Y. Wei, Z. Ren, A. Zhang, P. Mao, H. Li, X. Zhong, W. Li, S. Yang, and J. Wang, *Adv. Funct. Mater.* 28, 1706690 (2018).
61. H. Tang, J. Zhong, W. Chen, K. Shi, G. Mei, Y. Zhang, Z. Wen, P. Müller-Buschbaum, D. Wu, K. Wang, and X.W. Sun, *ACS Appl. Nano Mater.* 2, 6135 (2019).